Langmuir
Article
pubs.acs.org/Langmuir

Viscoelastic Modeling with Interfacial slip of a Protein Monolayer Electrode-Adsorbed on an Acoustic Wave Biosensor

Jonathan S. Ellis[†,‡,§] and Michael Thompson*[,†,‡]

[†]*Department of Chemistry, University of Toronto, 80 St. George Street, Toronto, Ontario M5S 3H6, Canada, and* [‡]*Institute for Biomaterials and Biomedical Engineering, University of Toronto, 164 College Street, Ontario M5S 3C9, Canada.* [§]*Present address Tyndall National Institute, Lee Maltings, University College Cork, Cork, Ireland.*

Received February 24, 2010. Revised Manuscript Received April 6, 2010

Transverse-shear mode acoustic wave devices have been used as real-time, label-free detectors of conformational shifts in biomolecules on surfaces. However, material changes in the biochemical monolayers and coupling between the substrate and the surrounding liquid make it difficult to isolate the desired signal, so an understanding of these phenomena is required. An important step in this understanding is knowledge of the material properties of the linker layer that attaches a biochemically selective molecule to the gold surface, in our case, neutravidin. With the goal of obtaining material properties for a neutravidin monolayer, for use in future studies, neutravidin adsorption to the gold surface of an acoustic wave biosensor is described as a viscoelastic monolayer using one-dimensional modeling. Neutravidin is described as forming hydrated, viscoelastic monolayers, and slip is allowed at all interfaces. An impedance model is numerically fit to experimental values using a two-parameter minimization algorithm and values for the shear modulus of the neutravidin monolayer, in agreement with literature values for similar proteins, are obtained. Slip is found on the electrode surface prior to neutravidin adsorption. These results will be used for future modeling studies involving this protein as a linker protein.

Introduction

The characterization of conformational and structural shifts in biomolecules is of great interest and importance in fundamental biochemistry and in allied fields, such as bioanalytical chemistry and drug discovery. The conformation of a biomolecule in a specific environment determines its function and interactions with other molecules, and plays an important role in many diseases. Recent examples include prion diseases such as spongiform encephalopathies, which are likely triggered by a conformational shift in native, harmless prions, upon exposure to a misshapen prion. Such changes in the tertiary structure of proteins can result in alterations of the material properties of these molecules. Over the years, many techniques have been developed for the detection of processes such as molecular folding in solution, including nuclear magnetic resonance spectroscopy,[1] circular dichroism,[2] and gel electrophoresis.[3,4] Additionally, protein folding can be predicted computationally using molecular dynamics simulations.[5,6]

The conformation of biomolecules on surfaces is also of particular interest because of its relevance to biocompatibility and biosensor technology. With respect to implants, the solid interface can induce harmful structural effects on a variety of biochemical macromolecules. Biosensor response can also depend on the conformation of a biochemical receptor imposed on the surface of a device. Accordingly, it is not surprising that significant attention has been paid to the study of biomolecules on surfaces. Example techniques employed for this purpose include atomic force microscopy (AFM),[7] surface plasmon resonance (SPR),[8,9] and scanning probe technologies such as the scanning Kelvin nanoprobe (SKN).[10−12] Both AFM and SKN offer high resolution over a large area, but they are not suited to real-time analysis. Of the methods mentioned above, only SPR offers real-time detection.

Acoustic physics has been recently proposed as a technology applicable for the detection of conformational shifts of biomolecules attached to surfaces, specifically in the form of the transverse shear mode acoustic wave device (TSM).[13,14] The TSM device, which offers sensitive, label-free, and online detection of biochemical interactions, has been applied widely in the field of bioanalytical chemistry in recent years.[13] Applications have included the detection of nucleic acid hybridization,[15] immunochemistry,[16] and protein interactions,[17,18] Furthermore, recent times have seen the sensor used to monitor the behavior of living cells on surfaces.[19−22] Traditionally, this device has often been

*Corresponding author. E-mail: mikethom@chem.utoronto.ca.

(1) Dyson, H. J.; Wright, P. E. *Annu. Rev. Phys. Chem.* **1996**, *47*, 369–395.
(2) Greenfield, N. J. *Anal. Biochem.* **1996**, *235*, 1–10.
(3) Goldenberg, D. P.; Creighton, T. E. *Anal. Biochem.* **1984**, *138*, 1–18.
(4) Righetti, P. G.; Verzola, B. *Electrophoresis* **2001**, *22*, 2359–2374.
(5) Karplus, M.; McCammon, J. A. *Nat. Struct. Biol.* **2002**, *9*, 646–652.
(6) van Gunsteren, W. F.; Hunenberger, P. H.; Mark, A. E.; Smith, P. E.; Tironi, I. G. *Comput. Phys. Commun.* **1995**, *91*, 305–319.
(7) Scheuring, S.; Fotiadis, D.; Möller, C.; Müller, S. A.; Engel, A.; Müller, D. J. *Single Mol.* **2001**, *2*, 59–67.
(8) Boozer, C.; Kim, G.; Cong, S.; Guan, H.; Londergan, T. *Curr. Opin. Biotechnol.* **2006**, *17*, 400–405.
(9) Robert, K. *J. Mol. Recog.* **2004**, *17*, 151–161.
(10) Cheran, L. E.; Chacko, M.; Zhang, M. Q.; Thompson, M. *Analyst* **2004**, *129*, 161–168.
(11) Cheran, L. E.; Sadeghi, S.; Thompson, M. *Analyst* **2005**, *130*, 1569–1576.
(12) Huo, H.; Cheran, L. E.; Thompson, M., Kelvin physics of protein layers printed in microarray format. In *New Approaches in Biomedical Spectroscopy*; Kneipp, K., Aroca, R., Kneipp, H., Wentrup-Byrne, E., Eds. American Chemical Society: Washington DC, 2007; pp 312−337.
(13) Cavic, B. A.; Hayward, G. L.; Thompson, M. *Analyst* **1999**, *124*, 1405–1420.
(14) Tsortos, A.; Papadakis, G.; Mitsakakis, K.; Melzak, K. A.; Gizeli, E. *Biophys. J.* **2008**, *94*, 2706–2715.
(15) Su, X. D.; Wu, Y. J.; Knoll, W. *Biosens. Bioelectron.* **2005**, *21*, 719–726.
(16) Zhang, J.; Su, X. D.; O'Shea, S. J. *Biophys. Chem.* **2002**, *99*, 31–41.
(17) Peh, W. Y. X.; Reimhult, E.; Teh, H. F.; Thomsen, J. S.; Su, X. D. *Biophys. J.* **2007**, *92*, 4415–4423.
(18) Stengel, G.; Hook, F.; Knoll, W. *Anal. Chem.* **2005**, *77*, 3709–3714.
(19) Braunhut, S. J.; McIntosh, D.; Vorotnikova, E.; Zhou, T.; Marx, K. A. *Assay Drug Dev. Technol.* **2005**, *3*, 77–88.
(20) Cheran, L. E.; Cheung, S. L.; Al Chawaf, A.; Ellis, J. S.; Belsham, D. D.; MacKay, W. A.; Lovejoy, D.; Thompson, M. *Analyst* **2007**, *132*, 242–255.
(21) Marx, K. A.; Zhou, T.; Montrone, A.; Schulze, H.; Braunhut, S. J. *Biosens. Bioelectron.* **2001**, *16*, 773–82.

considered to function as a gravimetric detector,[23] but it is now evident that the device operating in liquids is sensitive to many more factors than simple mass adsorption, such as film viscoelastic effects and interfacial slip. A significant challenge exists, however, in separating the mass response due to adsorption of an imposed monolayer, from that due to film mechanical properties, interfacial effects, and the presence of the buffer liquid.

The isolation of these effects is important in view of the fact that a number of recent studies have indicated that the TSM is capable of the detection of conformational shifts in biomolecules upon interaction with ligands known to induce such changes.[24−26] In all these studies, device signals were interpreted in terms of the perturbation of interfacial properties, contrary to the conventional gravimetric approach. However, these effects were only treated qualitatively and consideration of the mechanical properties of the biochemical film was omitted.

In the present paper, we consider previously reported experimental results for the adsorption of neutravidin to the bare gold electrode of the TSM device.[25] Neutravidin (NAv), the aglycosylated analogue of the protein avidin, is an important molecule in surface modification, because of its strong and irreversible binding to biotin, a 266-Da vitamin. The avidin−biotin interaction is commonly exploited for the attachment of biotinylated moieties to various substrates. With regard to the adsorption of neutravidin on the TSM sensor, consistently higher changes in series resonant frequency are observed that can be explained by the conventional mass deposition model. In this case, adsorption of the protein and binding of ligands are expected to lead to viscoelastic changes in the sensing layer, induced by the conformational change in the biomolecule.

Additionally, structural changes in the attached biochemical layer can lead to changes in coupling with the solvent, which in turn could result in interfacial slip. For a liquid under shear flow, slip occurs when the liquid particles directly adjacent to a surface have a finite velocity parallel to the surface. Slippage effects have been connected to hydrophobic surfaces under high hydrodynamic shear stress[27,28] and have been suggested as a possible explanation for anomalous results in acoustic wave biosensor studies.[29]

In this work, we consider a multilayer, one-dimensional model of the acoustic impedance of the biological system. Viscoelastic and interfacial effects are modeled at the surface−liquid interface, and the gold-neutravidin interface. The mechanical and coupling properties are numerically fitted to the experimental results using a perturbation analysis of the acoustic response. On the basis of an analysis of the frequency and resistance shifts obtained for the adsorption, we find that occurrence of the phenomenon of slip on the bare gold in liquid, prior to the addition of neutravidin, is a distinct possibility. Once adsorbed, neutravidin acts as a thin viscoelastic layer.

Theory and Background

The TSM Device as a Biosensor. The theory and application of acoustic wave devices as biosensors has been addressed in a number of reviews, and so will only be discussed briefly here. Such devices function through the generation of a resonant shear wave in an electroded quartz wafer. At the resonant frequency, the acoustic wave travels through the quartz with very little dissipation, and is reflected at the solid interface to maintain the standing wave. Changes at the substrate surface affect the apparent thickness and acoustic properties of the quartz wafer, and can be measured as changes in shear wave parameters.

When the device is used as a biosensor, measurements are generally performed in a liquid environment, which leads to energy dissipation at the surface−liquid interface and inertial storage. The limits of device functionality are (a) pure mass deposition and (b) viscous liquid adsorption. The former is characterized by a shift in the resonant frequency, described by the well-known Sauerbrey equation[30]

$$\Delta f = \frac{-2{f_0}^2}{Z_q} m_f \tag{1}$$

where f_s is the series resonant frequency, f_0 is the unloaded resonant frequency, $Z_q = 8.80 \times 10^5\ \mathrm{g \cdot cm^{-2} \cdot s^{-1}}$ is the characteristic acoustic impedance of quartz, and m_f is the mass per unit area of the adsorbed film.

In the latter, the inertial storage is described by a change in the resonant frequency, and the dissipation by either the motional resistance R_m, or the bandwidth Γ. For a viscous liquid, the sensor response in both f_s and R_m are proportional to the root of the density-viscosity product, as shown in the Kanazawa−Gordon description,[31,32]

$$\begin{aligned} \Delta f_{liq} &= \frac{-{f_0}^{3/2}}{Z_q\sqrt{\pi}}\sqrt{\rho_{liq}\eta_{liq}} \\ \Delta R_{liq} &= \frac{1}{8K^2C_0Z_q}\sqrt{\frac{\pi}{f_0}}\sqrt{\rho_{liq}\eta_{liq}} \end{aligned} \tag{2}$$

Here, $K^2 = 7.74 \times 10^{-3}$ is the electromechanical coefficient of quartz; C_0 is the parallel capacitance, approximately 10 pF; and ρ_{liq} and η_{liq} are the density and viscosity of the liquid. There is a dependence on the square-root of the density-viscosity product, with f_s and R_m changing in opposite directions. Dissipation can also be described by the bandwidth Γ. In some cases, this is more convenient, and depending on the situation, both R and Γ are used in this paper.

In biosensing applications, multiple layers must be considered, including the linker layer, the sensing layer, and the contacting liquid, shown schematically in Figure 1. Shifts in frequency and resistance are results of the absorption of each layer and are proportional to the change in the acoustic impedance due to adsorption. This change is often a combination of the limits described above. A general model to describe these changes is the small load approximation,[33−35] where the response is related to

(22) Wang, X. M.; Ellis, J. S.; Kan, C. D.; Li, R. K.; Thompson, M. *Analyst* **2008**, *133*, 85–92.
(23) Sheikh, S.; Blaszykowski, C.; Thompson, M. *Anal. Lett.* **2008**, *41*, 2525–2538.
(24) Lyle, E.-L. E. *Acoustic Coupling of Transverse Waves as a Mechanism for the Label-free Detection of Biomolecular Interactions*; University of Toronto: Toronto, Canada, 2004.
(25) Tassew, N. G. *Characterization of the HIV-1 TAR RNA-Tat Peptide and Drug Interactions by On-line Acoustic Wave Sensor*, Ph.D. Thesis, University of Toronto: Toronto, Canada, 2003.
(26) Wang, X. *Surface-attached Biomolecules and Cells Studied by Thickness Shear Mode Acoustic Wave Sensor*; University of Toronto: Toronto, Canada, 2008.
(27) Craig, V. S. J.; Neto, C.; Williams, D. R. M. *Phys. Rev. Lett.* **2001**, *8705*, 054504.
(28) Neto, C.; Craig, V. S. J.; Williams, D. R. M. *Euro. Phys. J. E* **2003**, *12*, S71–S74.
(29) Ferrante, F.; Kipling, A. L.; Thompson, M. *J. Appl. Phys.* **1994**, *76*, 3448–3462.
(30) Sauerbrey, G. *Z. Phys.* **1959**, *155*, 206–222.
(31) Kanazawa, K. K.; Gordon, J. G. *Anal. Chem.* **1985**, *57*, 1770–1771.
(32) Martin, S. J.; Granstaff, V. E.; Frye, G. C. *Anal. Chem.* **1991**, *63*, 2272–2281.
(33) Eggers, F.; Funck, T. *J. Phys. E: Sci. Instrum.* **1987**, *20*, 523–530.
(34) Johannsmann, D.; Mathauer, K.; Wegner, G.; Knoll, W. *Phys. Rev. B* **1992**, *46*, 7808–7815.
(35) Tessier, L.; Patat, F.; Schmitt, N.; Lethiecq, M.; Frangin, Y.; Guilloteau, D. *Sens. Actuators B* **1994**, *19*, 698–703.

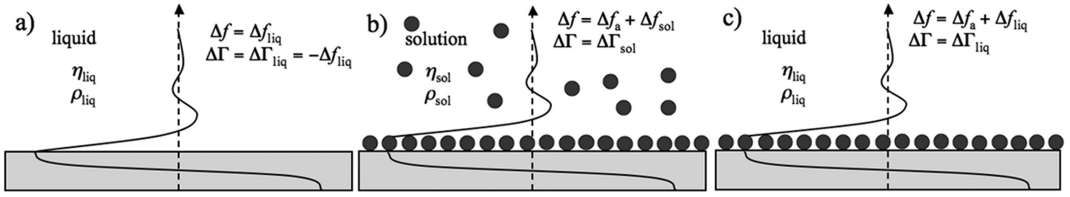

Figure 1. Theoretical representation of rigid thin-film adsorption from a viscous solution.

the lumped acoustic impedance of all layers in contact with the device surface. This is given by

$$\begin{aligned} \Delta f &= -\frac{f_0}{\pi Z_q}\mathrm{Im}(Z_L) \\ \Delta R_{liq} &= \frac{1}{8K^2 C_0 Z_q}\mathrm{Re}(Z_L) \end{aligned} \tag{3}$$

where Z_L is the combined acoustic impedance of the surface load. It can be described by the thicknesses and viscoelasticities of all the layers, including the semi-infinite liquid layer, and appropriate boundary conditions. For a purely viscous liquid, the change in bandwidth is equal and opposite to the change in frequency, as illustrated in Figure 1a.

Equation 3 only requires the combined load impedance to estimate the sensor response. The acoustic impedance of a single layer with thickness h_i and complex shear modulus G_i is[36,37]

$$Z_i = \sqrt{\rho_i G_i}\tanh(jk_i h_i) \tag{4}$$

The prefactor, $(\rho_i G_i)^{1/2}$, is the characteristic acoustic impedance of the layer and the wavenumber $k_i = \omega(\rho_i/G_i)^{1/2}$. Each layer combines to influence the load impedance, so the energy of any layer will be transferred to the device surface through all lower layers. The modeling technique for treating multiple layers is similar to that for a single layer, but each one has separate shear moduli and density, G_i and ρ_i.

Such a system, with combined solid film and liquid loading, has been solved by a number of researchers.[32,36,37] For a two-layer system, the load impedance can be approximated as[36,38]

$$Z_L = \frac{Z_1 + Z_2}{1 + \dfrac{Z_1 Z_2}{\rho_1 G_1}} \tag{5}$$

The Z_i are given by eq 4, where layer 1 is the layer directly contacting the device surface, and layer 2 is above that. It is important to note that the model described by eq 5 employs the no-slip boundary condition between each layer. In the sections below, we show that interfacial and slippage effects can be used to describe neutravidin adsorption. First, however, it is necessary to summarize the biophysical chemistry of the neutravidin molecule.

The TSM Device and Neutravidin−Biotin Surface Chemistry. For biosensor functionality, it is necessary to immobilize a surface linker to the gold electrode of the TSM to facilitate probe attachment. The gold−sulfur interaction has figured prominently in this respect, either through self-assembled thiol chemsitry[39] or the irreversible avidin (neutravidin)-biotin interaction.[40] In the second case, the sensing moiety is tagged with biotin for exposure to an adsorbed avidin monolayer.[41,42] This system has been employed successfully in a variety of acoustic biosensor applications such as immunochemistry,[43−46] detection of nucleic acid hybridization,[13,47−50] and protein interactions.[51−55] In many of these studies, nonadherence to the Sauerbrey[30] expression is evident.

Avidin is made up of 4 identical subunits, each with 128 amino acids, that form a globular shape with dimensions 60 × 55 × 40 Å and molecular weight 67 kDa.[40] It has high carbohydrate content, with approximately 10% of the weight composed of sugars, and is highly basic (pI = 9.5) so it is positive at neutral pH. Neutravidin is its aglycosolated analogue with the sugar side-chain removed. This molecule has neutral charge (pI = 6.3) and is smaller (60 kDa). Avidin and neutravidin both form monolayers on gold surfaces, with thicknesses of 48 Å for avidin[41] and approximately 42 Å for neutravidin.[42] From the dimensions of avidin, a close-packed monolayer would have surface coverage of approximately 7 pmol·cm^{-2}, although radio-labeling[50,56] and AFM[57] studies have shown that the actual coverage is on the order of 1−2 pmol·cm^{-2}.

Biotin is a water-soluble vitamin composed of an ureido ring fused with a tetrahydrothiophene ring attached to a valeric acid substituent. It has molecular mass of 244 Da and is approximately 10 Å long. Avidin has four biotin binding sites, one per subunit, so 4 mols of biotin bind stochiometrically per mole of avidin.[58]

(36) McHale, G.; Lucklum, R.; Newton, M. I.; Cowen, J. A. *J. Appl. Phys.* **2000**, *88*, 7304–7312.
(37) McHale, G.; Newton, M. I.; Banerjee, M. K.; Cowen, J. A. *Mater. Sci. Eng., C* **2000**, *12*, 17–22.
(38) Domack, A.; Prucker, O.; Ruhe, J.; Johannsmann, D. *Phys. Rev. E* **1997**, *56*, 680–689.
(39) Schreiber, F. *Prog. Surf. Sci.* **2000**, *65*, 151–257.
(40) Savage, M. D.; Mattson, G.; Surbhi, D.; Nielander, G. W.; Morgensen, S.; Conklin, E. J., *Avidin-Biotin Chemistry: A Handbook*; Pierce Chemical Company: Rockford, IL, 1992.
(41) Ebersole, R. C.; Miller, J. A.; Moran, J. R.; Ward, M. D. *J. Am. Chem. Soc.* **1990**, *112*, 3239–3241.
(42) Ghafouri, S.; Thompson, M. *Langmuir* **1999**, *15*, 564–572.
(43) Gizeli, E.; Liley, M.; Lowe, C. R.; Vogel, H. *Anal. Chem.* **1997**, *69*, 4808–4813.
(44) Hays, H. C. W.; Millner, P. A.; Prodromidis, M. I. *Sens. Actuators B* **2006**, *114*, 1064–1070.
(45) Storri, S.; Santoni, T.; Minunni, M.; Mascini, M. *Biosens. Bioelectron.* **1998**, *13*, 347–357.
(46) Tommoy, M.; Baer, R. L.; Spirasolomon, D.; Doherty, T. P. *Anal. Chem.* **1995**, *67*, 1510–1516.
(47) Dupont-Filliard, A.; Billon, M.; Livache, T.; Guillerez, S. *Anal. Chim. Acta* **2004**, *515*, 271–277.
(48) Furtado, L. M.; Thompson, M. *Analyst* **1998**, *123*, 1937–1945.
(49) Hianik, T.; Wang, X.; Andreev, S.; Dolinnaya, N.; Oretskaya, T.; Thompson, M. *Analyst* **2006**, *131*, 1161–1166.
(50) Su, H. B.; Kallury, K. M. R.; Thompson, M.; Roach, A. *Anal. Chem.* **1994**, *66*, 769–777.
(51) Hook, F.; Voros, J.; Rodahl, M.; Kurrat, R.; Boni, P.; Ramsden, J. J.; Textor, M.; Spencer, N. D.; Tengvall, P.; Gold, J.; Kasemo, B. *Colloid Surf. B* **2002**, *24*, 155–170.
(52) Lubarsky, G. V.; Davidson, M. R.; Bradley, R. H. *Biosens. Bioelectron.* **2007**, *22*, 1275–1281.
(53) Lyle, E. L.; Hayward, G. L.; Thompson, M. *Analyst* **2002**, *127*, 1596–1600.
(54) Wang, X.; Ellis, J. S.; Lyle, E. L.; Sundaram, P.; Thompson, M. *Mol. Biosyst.* **2006**, *2*, 184–192.
(55) Yang, M. S.; Thompson, M. *Anal. Chim. Acta* **1993**, *282*, 505–515.
(56) Furtado, L. M.; Su, H. B.; Thompson, M.; Mack, D. P.; Hayward, G. L. *Anal. Chem.* **1999**, *71*, 1167–1175.
(57) Nisman, R. *Immobilization and Characterization of Oligonucleotides on Functionalized Substrates*; University of Toronto: Toronto, Canada, 2002.
(58) Nardone, E.; Rosano, C.; Santambrogio, P.; Curnis, F.; Corti, A.; Magni, F.; Siccardi, A. G.; Paganelli, G.; Losso, R.; Apreda, B.; Bolognesi, M.; Sidoli, A.; Arosio, P. *Eur. J. Biochem.* **1998**, *256*, 453–460.

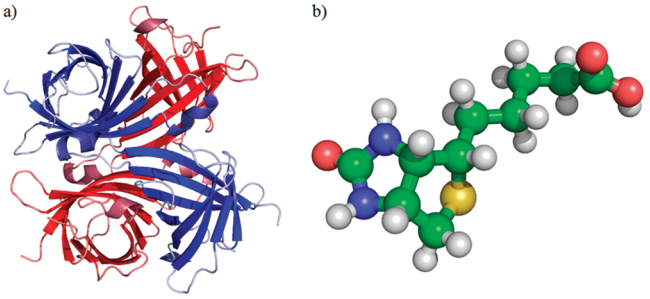

Figure 2. Molecular representations of (a) avidin and (b) biotin. Avidin (1RAV[58]) is in the biomolecular configuration, showing all four biotin binding subunits.

Molecular representations of avidin and biotin are shown in Figure 2.

Acoustic sensor responses for adsorption of neutravidin are on the order of −200 Hz, generally twice as large as the signals for adsorption of avidin, which are on the order of −100 Hz. The orientation of neutravidin will depend on the hydrophobic character of the gold surface, which will, in turn, affect its binding activity.[59] If the gold surface is hydrophobic (which is likely unless stringent cleaning protocols are used), then the hydrophobic domains of neutravidin will orient toward the surface, and the hydrophilic domains will be exposed, thus presenting a hydrophilic surface to the liquid. Because of the exposed hydrophilic domains, the protein layer will be hydrated, with liquid molecules penetrating into the protein layer. On a hydrophilic surface, neutravidin's hydrophilic domains will be oriented toward the surface, exposing the hydrophobic domains to the liquid.

Because neutravidin has no sugars and so would not spread out on the hydrophilic surface, thereby maintaining its biotin binding activity. As well, it would likely be more densely packed than avidin on the surface, as it would maintain its globular shape due to the lack of sugars. The hydrophilic domains would not be exposed, however, so there may be less hydration of the neutravidin layer on a hydrophilic surface than a hydrophobic one.

The gravimetric response for a close-packed neutravidin surface of 7 pmol·cm^{-2} would be −77 Hz, as predicted from eq 1. Instead, the observed frequency shift for avidin is generally −100 Hz, while that for neutravidin is as high as −200 Hz. Radiolabeling studies show a surface concentration on the order of 1.1 pmol·cm^{-2}, significantly less than close-packed.[25] The predicted gravimetric frequency response for this surface coverage of the 67-kDa avidin is on the order of −12 Hz (eq 1), and for the 60-kDa neutravidin, −11 Hz. The large discrepancy between the expected mass responses of the two molecules, which are similar, and the observed shifts, clearly indicates that the gravimetric model cannot adequately predict adsorption of these biomolecules in liquids, and an alternative model is required to interpret these results. Some authors have discussed trapped gas or nanobubbles at the device interface as a possible cause for the shifts,.[60] However, Tsionsky et al.[61] demonstrated experimentally that nanobubbles are not present under most conditions.

In addition to film viscoelastic effects outlined above, a possible candidate is slip at the surface−liquid interface. Slip and coupling effects have been described at solid−liquid interfaces, most notably for systems under high shear stress and for confined liquids. For a liquid under shear flow, slip occurs when the liquid particles directly adjacent to a surface have a finite velocity parallel to the surface. Recent work with aqueous flows at hydrophobic[62−65] and even hydrophilic[66−68] surfaces has shown that slip can occur at microscopic scales. Importantly, a number of authors have discussed the possibility of slip at the surface−liquid interface of an acoustic biosensor.[29,36,67,68] Since slippage depends on the surface−liquid affinity and surface morphology, biomolecular conformational changes due to binding of an analyte to a surface-immobilized moiety could lead to interfacial slip. These effects would influence acoustic wave propagation, making interpretation of the signal more difficult. Accordingly, the ability to predict the effects of slip is essential to the interpretation and understanding of signals obtained from biosensor devices based on acoustic physics.

Slip Theory. A complete discussion of slip theory is not required for this analysis, and has been covered in depth by others.[69−74] Instead, we concisely review some recent reports that have presented evidence for slip, and then consider slip models that will be used in this paper, as they pertain to acoustic wave devices.

Navier[75] proposed that partial slip was possible, and introduced the concept of a slip length. For a finite slip velocity v_s at the solid wall, the slip length b is an imaginary extrapolation length into the solid wall required to recover the no-slip condition, such that $v_s = b(\partial v_s/\partial n)_{z=0}$. A number of specific surface properties that govern boundary conditions have been considered extensively in the literature. These include wettability and substrate−liquid affinity,[67−69,74,76−84] hydrodynamic shear rate,[27,28,85−87] surface topology and roughness,[65,66,88−92] and surface material properties.[93−97]

(59) Huo, H. *Kelvin Physics of Substrate-attached Protein Layers and Protein Microarrays*; University of Toronto: Toronto, Canada, 2008.
(60) Theisen, L. A.; Martin, S. J.; Hillman, A. R. **2004**, *76*, 796−804.
(61) Tsionsky, V.; Kaverin, A.; Daikhin, L.; Katz, G.; Gileadi, E. *Phys. Chem. Chem. Phys.* **2005**, *7*, 1830–1835.
(62) Cho, J. H. J.; Law, B. M.; Rieutord, F. *Phys. Rev. Lett.* **2004**, 92.
(63) Pit, R.; Hervet, H.; Leger, L. *Tribol. Lett.* **1999**, *7*, 147–152.
(64) Tretheway, D. C.; Meinhart, C. D. *Phys. Fluids* **2004**, *16*, 1509–1515.
(65) Zhu, Y. X.; Granick, S. *Phys. Rev. Lett.* **2002**, *88*, 106102.
(66) Bonaccurso, E.; Butt, H. J.; Craig, V. S. J. *Phys. Rev. Lett.* **2003**, *90*, 144501.
(67) Bonaccurso, E.; Kappl, M.; Butt, H. J. *Phys. Rev. Lett.* **2002**, *88*, 076103.
(68) Cottin-Bizonne, C.; Jurine, S.; Baudry, J.; Crassous, J.; Restagno, F.; Charlaix, E. *Eur. Phys. J. E* **2002**, *9*, 47–53.
(69) de Gennes, P. G. *Langmuir* **2002**, *18*, 3413–3414.
(70) Ellis, J. S.; Thompson, M. *Phys. Chem. Chem. Phys.* **2004**, *6*, 4928–4938.
(71) Granick, S.; Zhu, Y. X.; Lee, H. *Nat. Mater.* **2003**, *2*, 221–227.
(72) Lichter, S.; Roxin, A.; Mandre, S. *Phys. Rev. Lett.* **2004**, *93*, 086001.
(73) Neto, C.; Evans, D. R.; Bonaccurso, E.; Butt, H.-J. r.; Craig, V. S. J. *Rep. Prog. Phys.* **2005**, *68*, 2859.
(74) Vinogradova, O. I. *Int. J. Miner. Process.* **1999**, *56*, 31–60.
(75) Navier, C. L. M. H. *Mem. Acad. R. Sci. Inst. Fr.* **1823**, *6*, 389–440.
(76) Barrat, J. L.; Bocquet, L. *Phys. Rev. Lett.* **1999**, *82*, 4671–4674.
(77) Baudry, J.; Charlaix, E.; Tonck, A.; Mazuyer, D. *Langmuir* **2001**, *17*, 5232–5236.
(78) Blake, T. D. *Colloids Surf.* **1990**, *47*, 135–145.
(79) Bocquet, L.; Barrat, J. L. *Phys. Rev. Lett.* **1993**, *70*, 2726–2729.
(80) Horn, R. G.; Vinogradova, O. I.; Mackay, M. E.; Phan-Thien, N. *J. Chem. Phys.* **2000**, *112*, 6424–6433.
(81) Israelachvili, J. N., *Intermolecular and Surface Forces*., 2nd ed.; Academic Press: London, 1991; p 450.
(82) Jabbarzadeh, A.; Atkinson, J. D.; Tanner, R. I. *J. Chem. Phys.* **1999**, *110*, 2612–2620.
(83) Pit, R.; Hervet, H.; Leger, L. *Phys. Rev. Lett.* **2000**, *85*, 980–983.
(84) Tolstoi, D. M. *Dokl. Akad. Nauk SSSR* **1952**, *85*, 1089–1092.
(85) Brochard, F.; de Gennes, P. G. *Langmuir* **1992**, *8*, 3033–3037.
(86) Leger, L.; Hervet, H.; Massey, G.; Durliat, E. *J. Phys.-Condes. Matter* **1997**, *9*, 7719–7740.
(87) Zhu, Y. X.; Granick, S. *Phys. Rev. Lett.* **2001**, *87*, 096105.
(88) Cottin-Bizonne, C.; Barrat, J. L.; Bocquet, L.; Charlaix, E. *Nat. Mater.* **2003**, *2*, 237–240.
(89) Daikhin, L.; Gileadi, E.; Katz, G.; Tsionsky, V.; Urbakh, M.; Zagidulin, D. *Anal. Chem.* **2002**, *74*, 554–561.
(90) Jabbarzadeh, A.; Atkinson, J. D.; Tanner, R. I. *Phys. Rev. E* **2000**, *61*, 690–699.
(91) McHale, G.; Newton, M. I. *J. Appl. Phys.* **2004**, *95*, 373–380.
(92) Ponomarev, I. V.; Meyerovich, A. E. *Phys. Rev. E* **2003**, *67*, 026302.
(93) Carre, A.; Gastel, J. C.; Shanahan, M. E. R. *Nature* **1996**, *379*, 432–434.
(94) Carre, A.; Shanahan, M. E. R. *Langmuir* **1995**, *11*, 24–26.
(95) Shanahan, M. E. R.; Carre, A. *Langmuir* **1995**, *11*, 1396–1402.
(96) Shanahan, M. E. R.; Carre, A. *J. Adhes.* **1996**, *57*, 179–189.
(97) Shanahan, M. E. R.; Carre, A. *C. R. Acad. Sci. Ser. IV-Phys. Astrophys.* **2000**, *1*, 263–268.

These considerations are discussed below in terms of acoustic sensing with biochemical surface modification.

Many studies have shown the existence of slip for nonpolar liquids such as alkanes. Migler et al.[98] used optical techniques to examine the local velocity of a polymer liquid near the wall and found large slip for weak polymer-surface interactions at high shear rates. Vinogradova[99] and Horn et al.[80] described the hydrodynamic forces of an ideal elastic fluid between two curved surfaces, and found slip lengths on the order of 30−50 nm. Molecular dynamics simulations of partially wetting liquids on a solid substrate wall found slip lengths on the order of 30 molecular diameters for weakly interacting liquids.[76]

Pit et al.[83] found direct experimental evidence of slip at a hexadecane/solid interface, for both polar and nonpolar surfaces, on the order of hundreds of nanometers. The authors also predicted that similar slip should occur on the surface of a TSM device.[63] Craig et al.[27] showed that slip occurs in an aqueous Newtonian liquid bounded by relatively hydrophilic surfaces, with slip length increasing with increasing shear rate. Similar results from Zhu and Granick[87] were achieved for spheres with nonpolar coatings immersed in tetradecane and water.

Slip and the Acoustic Wave Biosensor. Because of the high shear rates and small length scales involved in acoustic biosensor operation, it is highly likely that slip is possible at the surface liquid interface. It can be included by (i) a frictional stress in the shear stress balance between the surface and the liquid, or (ii) a slip parameter in the displacement/velocity boundary equation. Ferrante et al.[29] included slip in the displacement boundary equation between the surface and the liquid, with a complex slip parameter, α, so that

$$u_{liq,x}(z = h) = \alpha u_{q,x}(z = h) \tag{6}$$

where the $u_{i,x}$ are the particle displacements and h is the thickness of the quartz wafer. The no-slip condition is $\alpha = 1 + j0$, whereas for full slip, $\alpha = 0 + j0$, equivalent to the device operating in a vacuum. By fitting α to experimental data, the authors found values greater than 1.0 for both hydrophilic and hydrophobic surfaces. Hayward and Thompson[100] extended the slip parameter model to four layers, adding a purely elastic electrode layer and a viscoelastic polymer film. They allowed for complex slip at each interface, but the authors only included slip between the film and liquid. For α-type slip at the surface−liquid interface, the load impedance with slip is given by $Z_L^{slip} = \alpha Z_L^{no-slip}$, so the frequency and bandwidth shifts due to slip, are

$$\Delta f_{slip} = -\frac{f_0}{\pi Z_q}[\mathrm{Im}(\alpha Z_L^{NS}) - \mathrm{Im}(Z_L^{NS})] = \frac{f_0^{3/2}}{Z_q}\sqrt{\frac{\rho\eta}{\pi}}(1 - \alpha_R - \alpha_I)$$

$$\Delta\Gamma_{slip} = \frac{f_0}{\pi Z_q}[\mathrm{Re}(\alpha Z_L^{NS}) - \mathrm{Re}(Z_L^{NS})] = \frac{f_0^{3/2}}{Z_q}\sqrt{\frac{\rho\eta}{\pi}}(1 - \alpha_R + \alpha_I) \tag{7}$$

An analogous substitution could be made for slip at any interface.

Ellis and Hayward[101] showed mathematically that, for purely viscous liquids at an ideal elastic solid boundary, α is related to the real-valued slip length b by

$$\alpha = \exp\left(j\sqrt{2j}\frac{b}{\delta}\right) \tag{8}$$

Here, $\delta = (2\eta_{liq}/\omega\rho_{liq})^{1/2}$ is the penetration depth. This equivalency, however, is only strictly valid if the velocity profile is linear near the wall.[102]

Rodahl and Kasemo[103] used Stokes friction to equate the shear stresses in the liquid to the frictional stress of the liquid on the surface. Daikhin et al.[104] modeled slip between a rigidly coupled adsorbate and a liquid. Inclusion of slip resulted in extra frequency and bandwidth effects that are not equal and opposite, as would be the case for a change in the density or viscosity of the liquid. Du et al.[105] derived a model for heterogeneous slip by including a secondary flow field that depends on the Fourier components of the slip heterogeneity. While this model is still simply a parameter fit to the experimental data, it introduces an estimate for the device response if the surface heterogeneity is known. McHale et al.[36] used a similar description of slip, but modeled it at different layers using a slip parameter for layer i, $s_i = 1/k$. The acoustic load impedance for an adsorbed layer with slip at the adsorbate interface is

$$Z_L^{slip} = Z_L\left(\frac{1 + s_{liq}\dfrac{Z_aZ_{liq}}{Z_a + Z_{liq}}}{1 + s_{liq}\dfrac{Z_{liq}}{1 + Z_aZ_{liq}/(\rho_aG_a)}}\right) \tag{9}$$

where s is the slip parameter at the adsorbate-liquid interface, Z_a, ρ_a, and G_a are the acoustic impedance, density, and shear modulus of the adsorbate, Z_{liq} is the acoustic impedance of the liquid, and Z_L is the load impedance calculated without slip, from eq 5. Equation 9 can be used to estimate material and interfacial properties of biological adsorbate layers and biosensing from experimental data.

Ellis and Hayward[101] and McHale and Newton[91] showed that for a solid−liquid boundary condition, the slip coefficient s reduces to the slip length as $s_{liq} = b/\eta$. For single-valued parameters, Δf is less sensitive to the effects of slip than $\Delta\Gamma$, by a factor as high as 100. In cases involving amorphous biochemical monolayers, where a large amount of energy is being transferred or lost within a very thin layer, single-valued slip models may not be appropriate.

Slip at the gold surface prior to adsorption of neutravidin is likely because neutravidin does not bind well to highly hydrophilic surfaces[42,59] and the cleaning protocols used in the studies considered here would have resulted in mildly hydrophobic surfaces.[25,54] These results indicate that slip likely played a role, since the shifts in frequency are large compared to the changes in resistance. This is predicted from models for solid−liquid slip, where f_s is more sensitive to slip than R_m and Γ, and are discussed in the next section.

Modeling Approach and Results

The main model to be used is the small-load approximation, eq 3, as well as the various descriptions of slip considered above. Numerical fitting is performed using the fsolve tool from Octave 3.0.1. `fsolve` implements the MINPACK hybrd subroutine, which numerically finds a root for a system of N equations with N variables. A first-order matrix of partial derivatives is calculated by a forward-difference approximation.[106] All computations were

(98) Migler, K. B.; Hervet, H.; Leger, L. *Phys. Rev. Lett.* **1993**, *70*, 287–290.
(99) Vinogradova, O. I. *Langmuir* **1996**, *12*, 5963–5968.
(100) Hayward, G. L.; Thompson, M. *J. Appl. Phys.* **1998**, *83*, 2194–2201.
(101) Ellis, J. S.; Hayward, G. L. *J. Appl. Phys.* **2003**, *94*, 7856–7867.
(102) Willmott, G. R.; Tallon, J. L. *Phys. Rev. E* **2007**, *76*, 066306.
(103) Rodahl, M.; Kasemo, B. *Sens. Actuator A-Phys.* **1996**, *54*, 448–456.
(104) Daikhin, L.; Gileadi, E.; Tsionsky, V.; Urbakh, M.; Zilberman, G. *Electrochim. Acta* **2000**, *45*, 3615–3621.
(105) Du, B.; Goubaidoulline, I.; Johannsmann, D. *Langmuir* **2004**, *20*, 10617–10624.
(106) Moré, J. J.; Garbow, B. S.; Hillstrom, K. E., *User Guide for MINPACK-1*; Argonne National Laboratory: Argonne, IL, 1980; Vol. Report ANL-80−74.

performed on an Apple PowerMac G4 (Apple Inc., Sunnyvale, CA) running MacOS 10.4. All modeling calculations were performed using Octave 3.0.1.[107,108]

In this section, a variety of models are tested for the impedance of a neutravidin monolayer, to describe the adsorption of this protein on a gold surface. The models are evaluated by fitting to experimental data, and elucidate the physics of neutravidin monolayer formation and behavior. As well, these descriptions can explain results from similar experimental systems.

One set of experimental results that exploits the neutravidin−biotin interaction to immobilize the sensing surface is considered.[25] The measurement of neutravidin immobilization consisted of two states: the device response when the bare surface was operated in a buffer liquid, and the neutravidin-coated surface contacting the same buffer liquid. A solution containing neutravidin was introduced to the surface via a flow-injection system at low flow rates, so that the neutravidin was able to bind to the surface. After binding, the initial buffer solution was reintroduced to the system to remove any neutravidin molecules suspended in solution or not chemisorbed on the surface. In this way, the buffer liquid was the same as before neutravidin solution was introduced.

Throughout the experiments, the sensor signals f_s and R_m were measured, and the experimentally relevant values of $\Delta f = f_{\mathrm{NAv}} - f_0$ and $\Delta R = R_{\mathrm{NAv}} - R_0$ were determined. The device measured a change in the state of the surface from state 1, bare gold in contact with a liquid, to state 2, a neutravidin monolayer in contact with the liquid. Figure 3 shows an example of the signals measured by the device for neutravidin adsorption to the bare gold surface in buffer, monolayer formation, and subsequent washing. The average experimental responses on neutravidin adsorption were $\Delta f_{\mathrm{NAv}} = -180 \pm 16$ Hz and $\Delta R_{\mathrm{NAv}} = 1.8 \pm 0.4\ \Omega$. The errors are one standard deviation for 24 experimental runs.

Surface Concentration of Avidin and Neutravidin and Gravimetric Effects. Some authors model the binding of avidin or neutravidin to the TSM surface as purely gravimetric.[109,110] On the basis of the solution diameter of a neutravidin molecule of approximately 50 Å, full surface coverage would be 7 pmol·cm^{-2}. A purely gravimetric response would give a frequency shift of −77 Hz. In addition, full coverage is probably not achieved, due to steric and repulsive forces between the adsorbed biomolecules. This was demonstrated by AFM studies of neutravidin on mica surfaces, showing surface-bound avidin having a diameter of approximately 10 nm, yielding a 100 nm^2 area.[57] Assuming that the size of neutravidin on gold is similar to that of avidin on the functionalized mica surface, we would obtain a surface concentration of 1.6 pmol·cm^{-2}. This value is close to surface concentrations (1.1 pmol·cm^{-2}) detected by ^{32}P radiochemical labeling of RNA fragments binding to neutravidin immobilized to a gold surface.

There is obviously a huge discrepancy between the expected mass responses of the two molecules and their observed signals, indicating that the mass response model cannot adequately predict adsorption of these biomolecules.

Viscoelastic Model of Neutravidin Adsorption. A motivation for modeling the adsorption of a neutravidin film from the observed acoustic response is to obtain the material parameters of the monolayer. These parameters can then be used as a basis for modeling subsequent adsorption of sensing moieties, to explain the analyte response, and to compare similar systems. As well, such models may reveal some of the mechanisms for the shifts described above.

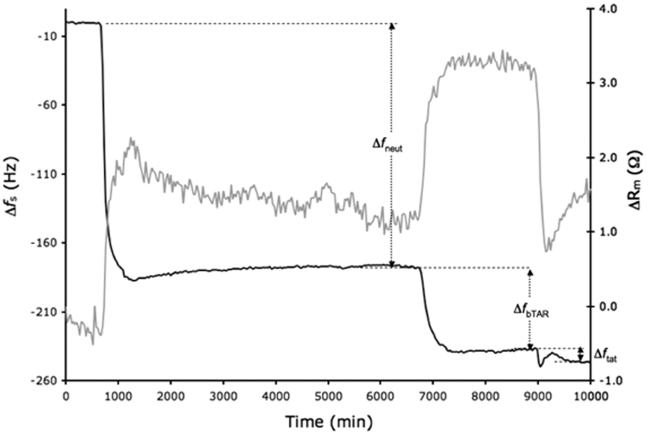

Figure 3. Sample plot of a single run from ref 25 showing Δf (black line) and ΔR (gray line) for neutravidin adsorption, bTAR immobilization, and *tat* binding. For clarity, only the frequency shifts are shown.

The model consists of describing the load impedance Z_L, which in this case has two layers: the neutravidin monolayer (viscoelastic film), in contact with the buffer (a semi-infinite viscous liquid). Neutravidin forms a 42-Å thick monolayer, so eq 5 can be used. The impedance model requires estimates for the model parameters before it can be solved, so it is important to obtain any known values of the system. The observations are shifts in f_s and R_m due to a perturbation of the system as it responds by changing from state 1, bare gold in liquid, to state 2, the neutravidin-coated surface. The system parameters can be predicted from the device response and the model equations (eqs 3 and 5) provided the correct form of the impedance Z_L is chosen. To facilitate analysis, the bandwidth $\Delta\Gamma$ is used instead of R_m. Any observed value of R_m is converted to an equivalent bandwidth.

Unfortunately, the data set for the initial state, the bare gold in contact with the buffer, was incomplete and the unloaded frequency f_0 and bandwidth Γ_0 are unknown. Consequently, we cannot determine the material properties of the bulk liquid from eq 2. However, since the buffer liquid properties do not vary between states 1 and 2, any change in the monolayer can be assumed independent of the liquid properties. As such, we set the buffer as an aqueous liquid with properties similar to water, so $\rho_{liq} = 1\ \mathrm{g\cdot cm^{-3}}$ and $\eta_{liq} = 1\ \mathrm{cP} = 10^{-2}\ \mathrm{g\cdot cm^{-1}\cdot s^{-1}}$. Provided the aqueous assumption is valid, any variation in Δf and $\Delta\Gamma$ are due exclusively to changes in the biochemical film or the interaction between the film and the liquid. Estimation of the unloaded frequency of the device f_0 is described in the Supporting Information.

To determine the density of the neutravidin monolayer, we assume that it is not uniformly packed, but instead is sparse and hydrated. If each molecule is evenly spaced on the surface and separated by 4 nm from its nearest neighbors, there would be a significant amount of water penetration into the monolayer. The crystal structure of avidin[58] shows that the molecular dimensions are 60 × 55 × 40 Å, so the area occupied by a molecule on the surface is assumed to be 33 nm^2. Since the known surface concentration is approximately 1−1.5 pmol·cm^{-2}, or approximately 100 nm^2/molecule, there is remaining 67 nm^2/molecule spacing that could be filled with water.

(107) Eaton, J. W., *GNU Octave Manual*; Network Theory Limited: Surrey, UK, 2002.
(108) Eaton, J. W. *Octave*, **2007**.
(109) Anzai, J.; Nakamura, N. *J. Chem. Soc., Perkin Trans. 2* **1999**, 2413–2414.
(110) Cosnier, S.; Perrot, H.; Wessel, R. *Electroanalysis* **2001**, *13*, 971–974.

The density of the neutravidin monolayer will be a combination of the densities of water and the neutravidin molecule itself, and a function of the relative surface concentrations of each. The dry surface density of neutravidin can be estimated from the molecular mass of the molecule and the known surface concentration. For avidin, the surface concentration has been determined at approximately 1.1 pmol·cm^{-2}.[42,111] Because of the absence of sugar groups on neutravidin, it likely is closer packed than avidin,[111] so an estimate of 1.5 pmol·cm^{-2} is more reasonable. The associated molecular area for this surface concentration is 100 nm^2, and the dry surface density is $\rho_{surf} = M_{NAv} \times c_{surf} = 96$ ng·cm^{-2}. The associated three-dimensional dry density can be found by dividing this result by the layer thickness, giving $\rho_{NAv,dry} = 0.23$ g·cm^{-3}.

The wet density can be estimated by assuming that the remaining volume is occupied by liquid molecules at the density of the liquid. For an aqueous liquid, the density would be close to that of water, so $\rho_{liq} = 1$ g·cm^{-3}. Therefore, the remaining area, 67 nm^2/molecule, is occupied by liquid molecules, so the density of the neutravidin monolayer is $\rho_{NAv} = \rho_{NAv,dry} + \rho_{liq} A_{un} N_A c_{surf}$, where ρ_{liq} is the density of the liquid, N_A is Avogadro's number, and A_{un} is the remaining unoccupied area per molecule. For $\rho_{liq} = 1$ g·cm^{-3} and $c_{surf} = 1.5$ pmol·cm^{-2}, the total density is $\rho_{NAv} = 0.87$ g·cm^{-3}. While this is a rough estimate, it should be suitable for this study.

This value is influenced by both the density of the molecule itself and the surface concentration and distribution on the surface. Essentially, the surface area is occupied by approximately half water and half neutravidin, and since the liquid density is much greater than the neutravidin, the liquid density dominates. This is an estimate, since the liquid will not behave like a solid mass within the monolayer but instead will have some viscous properties as well.

Viscoelasticity in the film is described using a simple linear model. A Kelvin−Voigt (KV) element is used as it is a good universal model. Higher-order models may be better-suited for biological description,[112] but since there are only two experimental values, any higher-order model can be reduced to the KV shear modulus, $G_f = G' + jG''$. For consistency, the parameters will be quoted in terms of KV shear modulus, $\mu + j\omega\eta$.

The change in state being modeled is characterized by changes in measured changes in frequency and resistance in Table 1. It is assumed that the neutravidin surface has a thickness of 4.2 nm, and a surface concentration of 1.5 pmol·cm^{-2}. The model impedance is given by eq 2 for the bare gold surface in liquid and eq 5 for the viscoelastic layer, with shear modulus $G_f = \mu_f + j\omega\eta_f$. An error analysis showing that a viscoelastic model cannot describe the adsorption of neutravidin is shown in the Supporting Information. Over a broad range of elastic and viscous shear moduli, the lowest relative error was 78%. If the surface coverage was varied, this only improved to 46%. The error analysis indicates that some other factor is affecting the frequency shift, very likely interfacial effects. To model neutravidin adsorption, interfacial coupling phenomena such as slip must be considered.

Effect of Interfacial Coupling Changes. Interfacial coupling changes are a likely source of the discrepancies in the results seen for the adsorption of neutravidin, for the reasons described above. Most importantly, the change in frequency on NAv adsorption is much larger than the accompanying change in dissipation, which is commensurate with single-valued slip models. We can include slip through the single-valued slip parameter s, with s_{liq} the slip value between the neutravidin-modified surface and the liquid. The actual impedance with slip is given by eq 9. A limitation of this model is that a guess for the viscosity is required, since there are only two experimental observations. A good initial guess of the viscosity is that of the liquid, $\eta_{NAv} = 0.01$ g·cm^{-1}·s^{-1}, since it is assumed that the protein is sufficiently hydrated. Using the `fsolve` function in Octave (v3.0.1), values of μ_{NAv} and s_{liq} were found that predicted the experimental values. These solutions are shown in Table 1.

Table 1. Initial Model Estimates of Viscoelasticity and Interfacial Slip[a] for Film Viscosity $\eta_{NAv} = 0.01$ g·cm^{-1}·s^{-1}

Δf/Hz	ΔR/Ω	log(μ_{NAv})	s_{liq} (× 10^{-5})	Δf/Hz	ΔR/Ω	log(μ_{NAv})	s_{liq} (× 10^{-5})
−175	1.38	6.23	−6.57	−208	2.30	5.88	−9.18
−170	0.99	6.37	−6.20	−189	1.61	6.14	−7.55
−162	1.73	6.13	−6.07	−157	1.48	6.19	−5.61
−214	1.82	6.02	−8.92	−165	3.40	-	-
−188	0.78	6.43	−7.14	−179	1.15	6.28	−6.74
−182	1.77	6.07	−7.35	−174	1.25	6.26	−6.52
−197	1.69	6.11	−7.72	−170	2.46	-	-
−205	2.12	5.92	−8.78	−218	2.44	-	-
−173	1.82	6.08	−6.84	−178	0.79	6.44	−6.54
−178	1.67	6.11	−7.04	−197	2.60	-	-
−181	1.86	6.04	−7.42	−176	1.47	6.19	−6.75
−164	1.54	6.18	−6.07	−187	2.40	-	-

[a] The units of μ_{NAv} are g·cm^{-1}·s^{-2} and for s, cm^2·s·g^{-1}. A dash indicates that the solver could not find a solution for the given parameters.

The results in Table 1 require some interpretation. The stiffness values appear reasonable, but solutions were not found for some of the observations, which can be attributed to the arbitrary estimation of the film viscosity at 10^{-2} g·cm^{-1}·s^{-1}. Also of interest are the negative values obtained for the slip, which indicates that coupling at the interface increases from state 1 to state 2. It could be caused by a *stick length*, whereby the affinity of the surface for the liquid is sufficiently strong and induces increased ordering in the contacting liquid, so that the position of zero velocity is moved into the liquid, instead of into the wall.[113] However, since in this formulation it is only the relative slip that is being modeled, a more likely explanation is that the liquid is slipping on the bare gold surface, with little or no slip upon neutravidin adsorption.

Before modeling this behavior, it is necessary to find solutions for all the experimental observations listed in Table 1. The problem lies in the assumption that $\eta_{NAv} = 10^{-2}$ g·cm^{-1}·s^{-1}, which is not valid for all the cases. Assuming that the general viscoelastic character of the neutravidin layer remains constant throughout the runs, we obtain an estimate of η_{NAv} from the fitted value of μ_{NAv}. The ratio of the shear viscosity to the shear stiffness is $\omega\eta/\mu = \omega\tau$ is a measure of the liquid or solid nature of the film. A value of $\omega\tau$ below 1 means that the elasticity dominates, and above 1 indicates a more viscous layer. We begin with a value of 0.5 as a reasonable estimate, although we could test multiple values to obtain a reasonable solution that works for all scenarios.

An appropriate value for η_{NAv} can be found by interpolation using a cubic spline algorithm. First, the model with slip is run for a range of η_{NAv} values. The values for each model solution are interpolated using the Octave `interp1` function with cubic spline interpolation to find η_{NAv} for the desired $\omega\tau$.

To model the negative slip behavior, state 1 becomes the slip case, and state 2, after neutravidin adsorption, is nonslip.

(111) Tassew, N.; Thompson, M. *Anal. Chem.* **2002**, *74*, 5313–5320.
(112) Wu, X. Y.; Levenston, M. E.; Chaikof, E. L. *Biomaterials* **2006**, *27*, 5315–5325.
(113) Persson, B. N. J., *Sliding Friction: Physical Principles and Applications*, 2nd ed.; Springer: Berlin, 2000; p 515.

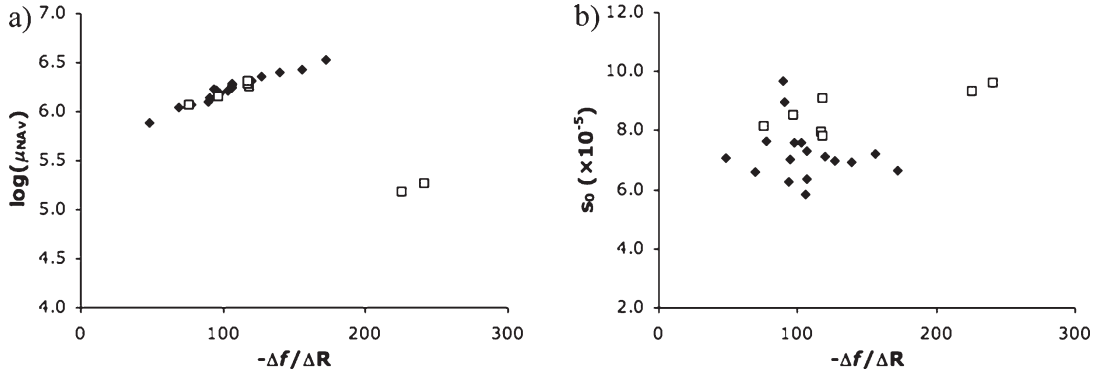

Figure 4. Neutravidin monolayer (a) stiffness $\log(\mu_{NAv})$ and (b) slip s_0 as they vary with the ratio $\Delta f/\Delta R$. The values were determined numerically from the experimental observations and eqs 5 and 10. Values of $\omega\tau = 0.3$ (♦) and 0.22 (□) were used.

The general equations for slip remain the same, except now slip occurs for the bare liquid, which is described by the following equation[36]

$$Z_L^{slip} = \frac{Z_{liq}}{1 + s_0 Z_{liq}} \tag{10}$$

where s_0 is the slip between the liquid and the bare gold. The impedance for state 2 is given by the thin-film approximation with no slip, eq 5. The model is run for $\omega\tau = 0.3$, although in some cases, a solution was only found for $\omega\tau = 0.22$. This was determined by trial and error. The average values found were $\log(\eta_{NAv}) = -2.0 \pm 0.1$, $\log(\mu_{NAv}) = 6.1 \pm 0.3$, and $s_0 = (8 \pm 1) \times 10^{-5}$ cm^2·s·g^{-1}, with errors indicating one standard deviation (logarithmic in the case of η and μ). These solutions are shown in Figure 4, which displays the monolayer properties as they vary with the ratio of Δf to ΔR. The full data set and model estimates are shown in the Supporting Information.

Of most interest are the slip values, which are all in the range $10^{-4} \pm 10^{-5}$ cm^2·s·g^{-1}. Since $s = b/\eta$, this corresponds to an average slip length of 8 ± 1 nm, which is similar to slip length values for hydrophobic gold.[27,28] The η_{NAv} values correspond well to that of the buffer, which is aqueous. This is expected, since the neutravidin layer is hydrated and will be affected by the presence of water. The shear stiffness of a thin biopolymer film is difficult to test, and there is a wide range of values for thin-film protein layer stiffness values. In a recent study, Lubarksy et al.[52] found shear moduli on the order of 10^7 for thin films of HSA on an acoustic biosensor at high humidity, which is within an order of magnitude for the shear stiffness values found here.

Discussion

Surface-bound NAv was modeled as a viscoelastic monolayer with a surface concentration of 1.5 pmol·cm^{-2}. However, the large experimental values for frequency shifts upon neutravidin adsorption could not account for this, so interfacial slip was included on the bare gold surface, prior to the introduction of neutravidin. This required the combination of the viscoelastic parameters, since the numerical fitting algorithm could only determine two independent parameters. We used a linear viscoelastic model based on a KV solid with $G = \mu + j\omega\eta$ and $\tau = \eta/\mu$, and assumed a value of $\omega\tau = 0.3$. We were able to fit a value of μ and from this, calculate a value of η. These results are compared to other protein adsorption studies using acoustic biosensors. $\omega\tau$ is the ratio of dissipation to storage in the film, so $\omega\tau = 0.3$ corresponds to a relatively solid-like layer.

When relating these viscoelastic parameters to values from the literature, the comparison should be done primarily with other acoustic biosensor studies of similar proteins. Shear moduli of protein monolayers are frequency-dependent, and should be compared at similar frequencies under shear. For this reason, we examine a number of TSM studies of protein and nucleic acid viscoelasticity studies. Weber et al.[114] modeled shear viscosities of adsorbed fibrinogen on a variety of biopolymer surfaces used in biomedical implants, and found values between 0.01 and 0.05 g·cm^{-1}·s^{-1}. Malmström et al.[115] described the adsorption of laminin to modified 5-MHz TSM surfaces and obtained a shear stiffness of 8×10^4 g·cm^{-1}·s^{-2} and shear viscosity of 2×10^{-2} g·cm^{-1}·s^{-1} for laminin on hydrophilic and hydrophobic surfaces. For patterned surfaces, they found values on the order of 5×10^5 g·cm^{-1}·s^{-2} and 3×10^{-2} g·cm^{-1}·s^{-1} for shear stiffness and viscosity, respectively. These correspond to $\omega\tau$ values of 7.8 and 1.9, which indicate more liquid-like layers, although the shear moduli are on the same order of magnitude as those found for NAv.

Dutta et al.[116] immobilized poly-L-lysine and histone on gold TSM surfaces and observed the viscoelastic changes in these monolayers due to cross-linking by glutaraldehyde. This led to a dehydration of the protein layer. Using a similar KV viscoelastic description, the authors found initial shear stiffness and viscosity of 2.5×10^6 g·cm^{-1}·s^{-2} and 3.0×10^{-2} g·cm^{-1}·s^{-1}, respectively, for PLL. For histone, these values were 1.2×10^5 g·cm^{-1}·s^{-2} and 1.3×10^{-2} g·cm^{-1}·s^{-1}. For the 5-MHz crystals used, these correspond to $\omega\tau$ values of 0.38 and 3.4, respectively. Comparing these results to our neutravidin model, the PLL shows similar behavior, in spite of being a much larger protein (300 kDa for PLL versus 60 kDa for NAv). Histone, on the other hand, which is approximately one-third the size of NAv, is less stiff and more viscous than the NAv layer. This is possibly due to the large amino acid tail of the histone molecule, which could lead to a large amount of hydration of the layer. Once cross-linking had occurred, the PLL layer stiffened to 2.5×10^7 g·cm^{-1}·s^{-2} and 17.5×10^{-2} g·cm^{-1}·s^{-1} and histone increased to 1.6×10^5 g·cm^{-1}·s^{-2} and 2.0×10^{-3} g·cm^{-1}·s^{-1}. This corresponds to $\omega\tau$ values of 0.22 and 3.9. It is interesting to note that cross-linking made the PLL monolayer more solid-like, whereas the histone layer became more liquid-like.

We obtained slip values of $s_0 = 8 \pm 1 \times 10^{-5}$ cm^2·s·g^{-1} for the bare gold surface. Recall that the slip model from eq 9 can be related to the slip length as $s_{liq} = b/\eta$, where η is the bulk viscosity,

(114) Weber, N.; Pesnell, A.; Bolikal, D.; Zeltinger, J.; Kohn, J. *Langmuir* **2007**, *23*, 3298–3304.
(115) Malmstrom, J.; Agheli, H.; Kingshott, P.; Sutherland, D. S. *Langmuir* **2007**, *23*, 9760–9768.
(116) Dutta, A. K.; Nayak, A.; Belfort, G. *J. Colloid Interface Sci.* **2008**, *324*, 55–60.

in our case $\eta_w = 0.01$ g·cm^{-1}·s^{-1}. Therefore, the experimental value for the slip length is on the order of 8 nm. This is comparable to other studies that have reported slip of Newtonian liquids on solid substrates using the surface force apparatus (SFA).[117] With this device, surfaces of various geometries immersed in liquid approach one another and the drainage force between the two surfaces is measured. Some surfaces can be modeled with the no-slip condition, whereas others require a slip boundary condition. This depends on shear rate, surface roughness, and the free energies of the surfaces. For water draining between a sphere and a flat surface of hydrophobic silanized Pyrex ($\theta = 100°$), a slip length of 100 nm was found.[68] However, the shear forces were extrapolated from data at large distances from the surface, so it is possible that the velocity gradient is very high close to the wall, but is not being detected. For a similar system (silanized glass surfaces), Cho et al.[62] found a slip length of 30 nm for water, and determined that onset of slip was dependent on the liquid dipole moment, for nonwetting liquids. Craig et al.[27,28] observed slip lengths between 0 (no-slip) and 8 nm for aqueous sucrose solutions draining from the space between a gold surface and an approaching gold sphere, both coated with alkyl−thiol SAM surfaces. Higher slip lengths were found at higher shear rates.

The cases considered above involve measurements of slip and surface coupling on gold and other surfaces using SFA detection. While these measurements provide a good context for comparison of slip values, the actual quantities and conditions are different for high-frequency oscillating systems. We therefore consider actual values of slip calculated for the TSM surface, not simply models. However, in many cases the quoted slip values are relative or qualitative, as it is not possible to determine quantitative slip values from TSM measurements. Ferrante et al.[29] modeled slip with the complex slip parameter α for hydrophilic- and hydrophobic-coated TSM devices in glycerol. They found very high slip magnitudes for glycerol solutions in water (up to $|\alpha| = 5.5$ for pure water) with large slip angles as well. As discussed above, slip magnitude values larger than 1 correspond to the no-slip condition, and values less than one correspond to some decoupling at the interface. While no quantitative conclusions could be made, the authors did observe a decrease in slip magnitude with increasing viscosity, and slippage ($|\alpha| < 1$) for high glycerol content (high viscosity) solutions. Hayward and Thompson[100] found similar behavior, although their values for water on the bare gold surface were lower than ref 29.

Daikhin et al.[104] found slip lengths of up to 10 Å for aqueous solutions of $LiClO_4$ and pyridine. Higher slip lengths were found for higher surface excesses of pyridine on the gold surface, as controlled by electrochemical methods. Ellis and Hayward[101] studied different liquids on modified surfaces with the TSM and, for water, found slip lengths of 20 nm on bare, hydrophobic gold, and 75 nm for hydrophobic, alkyl−thiol modified gold surfaces (hexadecanethiol and butanethiol). There was a large discrepancy for the bare gold surface, which could have been due to inconsistent cleaning on the bare gold. These slip lengths correspond to α values of 0.9 (bare gold), 0.65 (hexadecanethiol), and 0.68 (butanethiol). Du et al.[105] modeled slip on heterogeneously patterned surfaces, and found rms slip lengths of between 9.5 and 11 nm for water on hydrophobic bare gold surfaces.

The modeling values we obtained for neutravidin adsorption appear to be consistent with other proteins that have been tested. While avidin derivatives have not been explicitly modeled, the shear stiffness values we found are within the range of 10^5 to 10^7 g·cm^{-1}·s^{-2} and the shear viscosity is near 10^{-2} g·cm^{-1}·s^{-1}, in close agreement with similar layers. The slip length values of approximately 8 nm for the bare gold surface are in agreement with inferred slip values from the SFA literature and TSM studies on similar surface. Most of the results are within an order of magnitude.

While there is good agreement between the viscoelastic and slip values computed in the present paper and literature, it is important to note that these models require a large number of fitting parameters. These include the quartz parameters, the liquid properties, and the film density and viscosity. As a result, the calculated solutions will be sensitive even to small errors in the fitting parameters. This will affect both the reliability of the fitted solutions and the reproducibility of values between separate experiments. A sensitivity analysis was not performed for the present study, and associated errors in the parameters could quantitatively influence the results reported herein. However, we believe that this work does indicate that purely viscoelastic effects cannot describe the system, and interfacial coupling and slippage are important factors in experiments of oscillating systems at high shear rates. These effects should not be ignored, especially when considering biochemical systems.

Conclusions

We have shown that interfacial slip can describe adsorption of a globular protein in cases where gravimetric and viscoelastic models alone cannot explain the acoustic signals. These treatments of interfacial slip and viscoelastic properties of proteins acids are comparable, within an order of magnitude, to similar systems found in the literature. This type of quantitative modeling of interfacial coupling involving biomolecules immobilized on acoustic biosensor has not been performed before.

There have been many experimental descriptions of viscoelastic changes in biological adsorbate layers on acoustic sensor surfaces.[17,18] However, none of these has included slip at any interface, in spite of mounting evidence that interfacial coupling should be considered. While studies have treated hydration of proteins,[52,118] none have discussed the large unexpected shift for avidin and neutravidin in terms of slippage on the bare gold.

For neutravidin binding, we determined that the slip length on bare gold in buffer to be 8 ± 1 nm, which is in agreement with other studies of slippage effects on gold surfaces in Newtonian liquids. The average KV shear stiffness and viscosity for the neutravidin layers were found to be $\mu_{NAv} = 1.2 \times 10^6$ g·cm^{-1}·s^{-2} and $\eta_{NAv} = 1 \times 10^{-2}$ g·cm^{-1}·s^{-1}, respectively. However, further study is required to clarify the interfacial characteristics of a gold surface in buffer, as well as adsorption of NAv, and to improve upon the precision of the slippage, shear properties, and conformational changes of the systems considered in this study.

This work is novel for a number of reasons. First, it presents viscoelastic and interfacial properties for comparison with other studies of biological monolayers on acoustic devices, especially involving modified surfaces. It is important to note that we have not created a sensor to measure slip and coupling changes. However, we have treated this physical phenomenon in a system where it likely has a significant effect on the device response. The quantitative material properties established in this work will

(117) Vinogradova, O. I. *Langmuir* **1998**, *14*, 2827–2837.

(118) Su, X.; Zhang, J. *Sens. Actuators B* **2004**, *100*, 309−314.

provide a framework for future analysis of systems involving neutravidin, as well as for the study of multilayered biochemical systems.

Acknowledgment. The authors gratefully acknowledge financial support of this work from the Natural Sciences and Engineering Research Council of Canada. J.S.E is grateful to an Ontario Graduate Scholarship and a Victoria Noakes Ontario Graduate Scholarship in Science and Technology for financial support. Discussions with G. Hayward at the University of Guelph (Guelph, Canada) and M. Urbakh and L. Daikhin at Tel Aviv University (Tel Aviv, Israel) proved immensely valuable.

Supporting Information Available: Text giving the estimation of unloaded frequency and error analysis for the viscoelastic response (including a figure showing the error) and a table giving the full data set and model estimates of viscoelasticity and interfacial slip for neutravidin monolayer. This material is available free of charge via the Internet at http://pubs.acs.org.